RSC Advances

PAPER

View Article Online
View Journal | View Issue

Cite this: *RSC Adv.*, 2025, **15**, 2766

Synergistic effects of *Uncaria gambir* and zinc oxide in polyvinyl alcohol films for enhanced UV and blue light shielding, antimicrobial properties, and hydrophobicity: improving application performance in sustainable packaging and protective eyewear

Dieter Rahmadiawan,[ab] Hairul Abral,*[cd] Muhammad Aldi Pratama,[c] Hyun-Joong Kim,[ef] Razan Muhammad Railis,[g] Robi Kurniawan,[h] Sri Rizki Putri Primandari,[b] Shih-Chen Shi[a] and Melbi Mahardika[di]

This study investigates the development and characterization of a novel composite material consisting of polyvinyl alcohol (PVA) integrated with *Uncaria gambir* (UG) and zinc oxide (ZnO) as fillers. The synergistic effects of UG and ZnO were investigated, focusing on their ability to enhance the film's properties. UV-vis spectrophotometry demonstrated that the composite film effectively blocked all UV (UV-A and UV-B) and blue light wavelengths. The mechanical properties were significantly enhanced, with tensile strength improving by 56% and elasticity by 38% compared to pure PVA. Additionally, water contact angle measurements showed an increase from 34.4° for pure PVA to 84.4° for the PVA/UG/ZnO composites, indicating a substantial improvement in hydrophobicity, which suggests the potential for extended application in environments where moisture resistance is crucial. These findings illustrate the potential of utilizing natural extracts and metal oxides in polymer composites for applications that require durable and effective protection against photodegradation and environmental factors. This study establishes a foundation for further exploration into biocompatible and environmentally sustainable materials with enhanced protective properties.

Received 16th December 2024
Accepted 14th January 2025

DOI: 10.1039/d4ra08801h

rsc.li/rsc-advances

1. Introduction

In the digital age, the extensive use of devices emitting blue light has escalated concerns regarding its potential health impacts. Blue light, a high-energy component of the visible spectrum with wavelengths ranging from 400 to 495 nm, can penetrate deeper into the eye than other forms, potentially leading to retinal damage and accelerating ocular aging.[1–4] Concurrently, exposure to ultraviolet (UV) light, which has wavelengths ranging from 280 to 400 nm and is naturally regulated by atmospheric conditions, remains a significant risk factor for skin damage, premature aging, and various forms of skin cancer.[5] These risks highlight the critical need for effective protective solutions, particularly in material development for shielding applications against these harmful rays. Given the growing concerns about environmental sustainability, there is an increasing demand for materials that are not only effective but also environmentally friendly and sustainable.[6–10] Modern advancements in material science have prioritized solutions that minimize environmental impact while maintaining high performance.

[a]*Department of Mechanical Engineering, National Cheng Kung University (NCKU), Tainan, Taiwan*

[b]*Department of Mechanical Engineering, Universitas Negeri Padang, Padang 25173, West Sumatera, Indonesia*

[c]*Laboratory of Nanoscience and Technology, Department of Mechanical Engineering, Andalas University, Padang 25163, West Sumatera, Indonesia. E-mail: abral@eng.unand.ac.id*

[d]*Research Collaboration Center for Nanocellulose, BRIN-Andalas University, Padang 25163, West Sumatera, Indonesia*

[e]*Research Institute of Agriculture and Life Sciences, Seoul National University, Gwanak-ro 1, Gwanak-gu, Seoul 08826, Republic of Korea*

[f]*Department of Agriculture, Forestry and Bioresources, Seoul National University, Gwanak-ro 1, Gwanak-gu, Seoul 08826, Republic of Korea*

[g]*Department of Industrial Engineering, Institut Teknologi Batam (ITEBA), Batam, Indonesia*

[h]*Department of Physics, Faculty of Mathematics and Natural Sciences, Universitas Negeri Malang, Jl. Semarang No. 5, East Java, 65145, Indonesia*

[i]*Research Center for Biomass and Bioproducts, National Research and Innovation Agency of Indonesia (BRIN), Cibinong, Indonesia*

Polyvinyl alcohol (PVA) stands out in the field of polymer science owing to its exceptional film-forming capabilities, biocompatibility, and water solubility, making it an excellent base for developing advanced materials.[11,12] Its inherent properties of clarity and flexibility enable wide-ranging applications, from packaging films to medical devices, thus providing an ideal matrix for composite materials aimed at protective coatings.[13,14]

Uncaria gambir (UG), derived from various plant sources, is prized for its antioxidant properties, which have been utilized in traditional medicine and as natural additives in food and cosmetics.[15,16] The incorporation of UG into material composites can leverage these antioxidant properties to stabilize against oxidative stress and enhance the durability of materials exposed to sunlight and other sources of radiation, such as UV light.[17] However, while PVA/UG composites exhibit some protective capabilities, they primarily offer limited shielding against UV light alone.[17] This specificity means that other harmful wavelengths, such as blue light, which are also detrimental to materials and can accelerate degradation processes, are not adequately addressed by PVA/UG composites. Additionally, although UG alone has some antibacterial properties, these are not sufficiently strong for applications that require higher antibacterial effectiveness.[18] To achieve more comprehensive protection, an additional approach is necessary.

Zinc oxide (ZnO) is another versatile agent known for its ability to block UV light, along with its antibacterial and antifungal properties.[19,20] In various applications, from sunscreens to semiconductor devices, ZnO has demonstrated efficacy in providing UV protection and enhancing the mechanical strength and thermal stability of composites.[21] Its non-toxicity and compatibility with other materials make it an ideal choice for a wide range of technological and medical applications.[22,23] Studies have demonstrated that ZnO nanoparticles can enhance mechanical properties, thermal stability, barrier performance, and antimicrobial activity in nanocomposites, as reported in various literature sources.[24–27] For instance, ZnO nanoparticles embedded in gelatin films improved their water vapor permeability by about 8.54%.[28] Similarly, the addition of ZnO to gelatin/cellulose nanofiber films resulted in enhanced tensile strength and antibacterial activity, demonstrating their potential as active food packaging materials.[29]

Moreover, ZnO is added to enhance barrier properties, particularly addressing the hydrophilic nature of UG, which can otherwise reduce the effectiveness of the barrier against moisture and other environmental factors.[30] Previous studies have shown that mixing UG with PVA results in increased antibacterial resistance, UV protection, heat resistance, tensile strength and so on.[31] However, the addition of UG alone to PVA does not significantly enhance antimicrobial properties.[32] Previous studies have shown that the addition of ZnO nanoparticles to PVA produces UV-light-resistant PVA/ZnO composites with excellent transparency and antibacterial properties.[33,34] Therefore, in this paper, we look more closely at the use of ZnO nanoparticles to prepare and characterize PVA/UG/ZnO composite films with better properties, providing more thorough knowledge of their behavior.

This study integrates UG and ZnO into a PVA matrix, marking the first investigation of the synergistic effects of these fillers within a PVA composite film. Our research focuses on significantly enhancing the composite's ability to block harmful light, exploring the comprehensive optical properties and protective efficacy of this novel material. We hypothesize that the dual functionality of UG and ZnO not only offers superior protective properties but also supports the objectives of sustainability and environmental safety in material production. By showcasing the enhanced optical characteristics and effectiveness of this PVA-based composite, our study lays the groundwork for future applications in areas such as protective eyewear and biodegradable packaging solutions that demand robust protection against light-induced degradation.

2. Materials and methods

2.1 Materials

Pure PVA (MW: ~75 000 g mol^{-1}, >99% hydrolysis) and ZnO nanoparticles with particle sizes less than 100 nm were supplied by Sigma-Aldrich Pte. Ltd Singapore. UG was obtained from the Sumatran Biota Laboratory, Andalas University, Padang. It was composed of catechins (91.8%), water (8.1%), and ash (0.1%). Sodium hydroxide (NaOH), sodium hypochlorite (NaClO), and sodium bromide (NaBr) were purchased from PT. Brataco, Padang, Indonesia. 2,2,6,6-Tetramethylpiperidine-1-oxyl (TEMPO) was acquired from Sigma-Aldrich Co., USA.

2.2 Sample preparation

The preparation of PVA/UG/ZnO composites commenced with the dispersion of PVA powder in water to form a 10 wt% solution, which was continuously stirred at 100 °C for 2 hours using a magnetic stirrer. After the PVA had completely dissolved, 1 wt% UG was added to the mixture, and stirring continued until full dispersion was achieved. Subsequently, ZnO was introduced at varying concentrations (0.02, 0.05, 0.07, and 0.1 wt%), and the mixture was stirred for an additional 30 minutes to ensure uniform distribution of ZnO particles throughout the composite. To further homogenize the mixture and break down any agglomerates, the solution was sonicated using an ultrasonic probe at 650 W for 15 minutes. The final mixture was then cast into a Petri dish and dried in an oven at 50 °C for 24 hours, resulting in the formation of solid films. Fig. 1 shows the photographs of the fabricated films for all samples.

2.3. Structural and chemical characterization

For the structural and chemical characterization of the samples, Fourier-transform infrared (FTIR) spectroscopy was conducted using a PerkinElmer Frontier FTIR spectrometer (PerkinElmer, Inc., USA). The spectra were recorded over the 4000–500 cm^{-1} range with a resolution of 4 cm^{-1}, and an average of 32 scans was taken for each sample. X-ray diffraction (XRD) analysis was performed using a PANalytical X'Pert PRO diffractometer (Philips Analytical, Netherlands), with Cu Kα radiation ($\lambda = 1.5406$ Å) at an operating voltage of 40 kV and a current of 30 mA. The

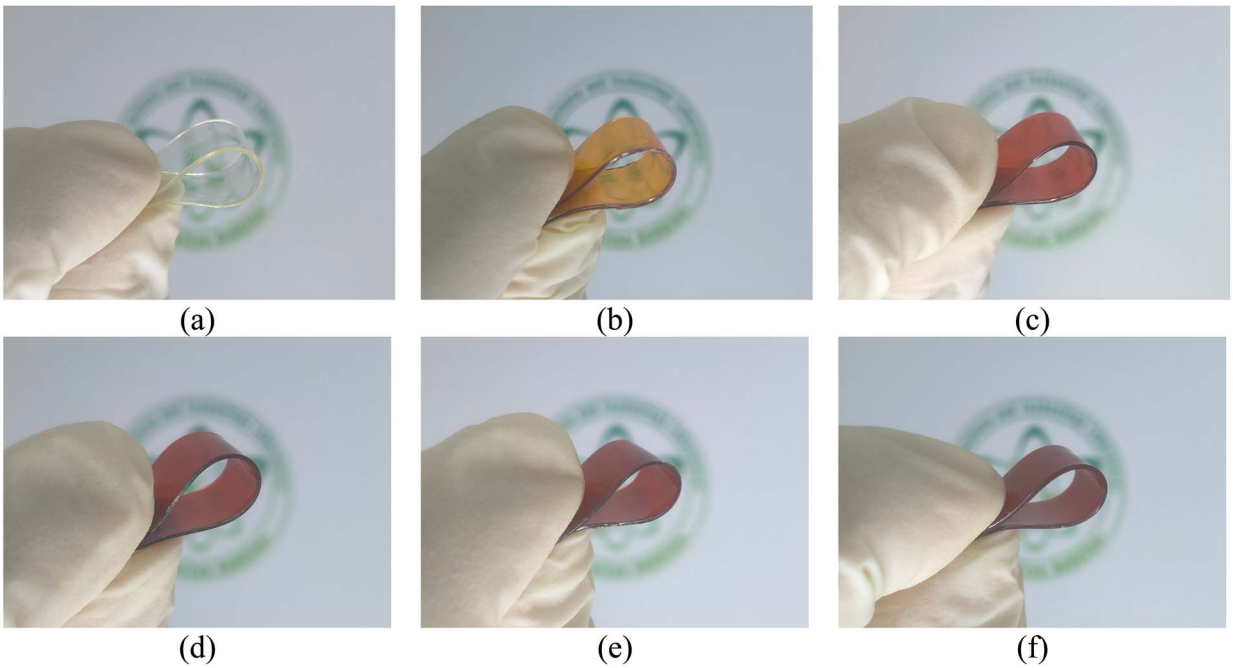

Fig. 1 Photographs of PVA (a), PVA/UG (b), PVA/UG/Z0.02 (c), PVA/UG/Z0.05 (d), PVA/UG/Z0.07 (e), and PVA/UG/Z0.1 (f).

diffraction patterns were collected over a 2θ range of 5–100° at a scanning rate of 1° min^{-1}. Thermogravimetric analysis (TGA) was carried out using a DTG-60 instrument (Shimadzu, Kyoto, Japan), serial number C30565000570, equipped with a TA-60WS thermal analyzer, FC-60A flow controller, and TA-60 software. Approximately 10 mg of each sample was placed into the instrument, which was set to a nitrogen atmosphere at a flow rate of 50 mL min^{-1}, and the samples were heated from room temperature to 600 °C at a rate of 20 °C min^{-1} to determine the thermal stability and degradation profiles.

2.4. Optical properties and surface characteristics

For the optical properties and surface characteristic analysis, UV-visible (UV-vis) spectroscopy was conducted using a Shimadzu UV 1800 spectrophotometer (Shimadzu, Japan) to measure the optical absorbance and transmittance of the composite films. The absorbance spectra were recorded in the range of 280–800 nm. The contact angles were measured using the ASTM D7334 methodology and the sessile drop method. A droplet of 10 μl of deionized water was placed on a representative spot outside the veneering area of the film. A digital microscope with an optical axis horizontal and parallel to the sample surface was used to measure the contact angle. The measurement was recorded 60 seconds after the droplet made contact with the surface, ensuring a stable reading, and all measurements were conducted at room temperature. For each film, one measurement was performed, with the droplet placed at the center of the film to maintain consistency across the samples.

2.5. Mechanical properties

The mechanical properties of the composite films, including tensile strength, Young's modulus, and elongation at break, were investigated using a Com-Ten 95T series universal testing machine in accordance with ASTM D638-Type V. The tests were conducted to evaluate the film performance under stress and to determine their mechanical behavior. The fractured surfaces of the films, obtained after tensile testing, were analyzed using Field Emission Scanning Electron Microscopy (FESEM) conducted with the ThermoFisher Dual-Beam FIB Aquilos2, equipped with a field-emission electron source, operating at room temperature. The samples were transferred under a vacuum from the preparation station to the Aquilos2 main chamber. To improve surface conductivity, a thin platinum layer of approximately 5 nanometers thick was deposited on the samples using an integrated retractable sputter coater, operating at 30 mA for 15 seconds. High-resolution imaging was achieved with an electron beam set to 25 pA and 2 kV.

2.6. Barrier and environmental resistance

The barrier properties of the composite films against moisture were assessed by measuring the water vapor permeability (WVP) using the gravimetric method in accordance with ASTM E96. A Water Vapor Transmission Rate Tester Machine (Labthink, China) was used to determine the vapor transmission rate of the samples. All tests were conducted at a temperature of 38 °C, with a differential relative humidity (RH) of 90% across the two sides of the samples. The moisture absorption (MA) of the films was measured using a previously described method. The film samples were first dried in a drying oven (Memmert, Germany, Model 55 UN) at 50 °C until they reached a constant weight. After drying, the films were placed in a closed chamber with a controlled RH of 75% at 25 °C. The samples were weighed every 30 minutes for 7 hours using a precision balance (Kenko, with 0.1 mg accuracy) to track the weight gain due to moisture absorption.

2.7. Durability and environmental impact

The durability and environmental impact of the composite films were evaluated through a soil burial test and antibacterial testing. For the biodegradability assessment, a soil burial test was conducted to track the degradation profile of the films over time. The samples were buried in natural soil at a depth of 10 cm and maintained under ambient conditions. The weight loss of the films was measured at regular intervals for 30 days to determine the rate and extent of biodegradation. The degradation profile provided insights into the environmental friendliness of the composite materials. The antibacterial properties of the films were assessed against *Staphylococcus aureus* (*S. aureus*) and *Escherichia coli* (*E. coli*) to determine their potential for antimicrobial applications. The antibacterial effectiveness was evaluated using a zone of inhibition method, in which the films were placed on agar plates inoculated with *S. aureus* and *E. coli*. The plates were incubated at 37 °C for 24 hours, and the inhibition zone around the samples was measured to determine the antibacterial activity.

3. Results and discussions

3.1 Optical properties and surface characteristics

Fig. 2a presents the FTIR spectra of PVA and PVA/UG/ZnO composite films across the various formulations. The spectra highlight the characteristic bands, particularly in the OH stretch region around 3200 cm^{-1}.[35] In the base PVA film, the OH stretch appears at 3270 cm^{-1} with 53.3% transmittance, indicating the presence of hydroxyl groups.[17] Upon the addition of UG, the intensity of the OH band decreases slightly to 3245 cm^{-1} with 58.5% transmittance, suggesting some interaction between PVA and UG, which affects the hydrogen bonding within the matrix. This interaction likely involves the formation of new bonds between PVA and the phenolic compounds in UG, which could slightly reduce the number of free OH groups.[17] This is similar to previous results.[31]

As ZnO is incrementally added to the PVA/UG mixtures, there is a notable decrease in the intensity of the OH band, shifting from 59.1% transmittance at 0.02 wt% ZnO to 68.6% transmittance at 0.1 wt% ZnO. This trend suggests that ZnO has a significant impact on the hydrogen bonding environment within the composite. The increase in transmittance and the shift in the OH band peak could be attributed to the interaction of ZnO particles with the OH groups of PVA and UG, potentially forming Zn–OH bonds.[36] This interaction leads to a reduction in the availability of free OH groups, thus diminishing the overall intensity of the OH band.

Furthermore, the wavelength region of 1000–1100 cm^{-1} presents the C–O stretch. This peak, indicating ether or alcohol groups, exhibits a decrease in intensity after the addition of UG

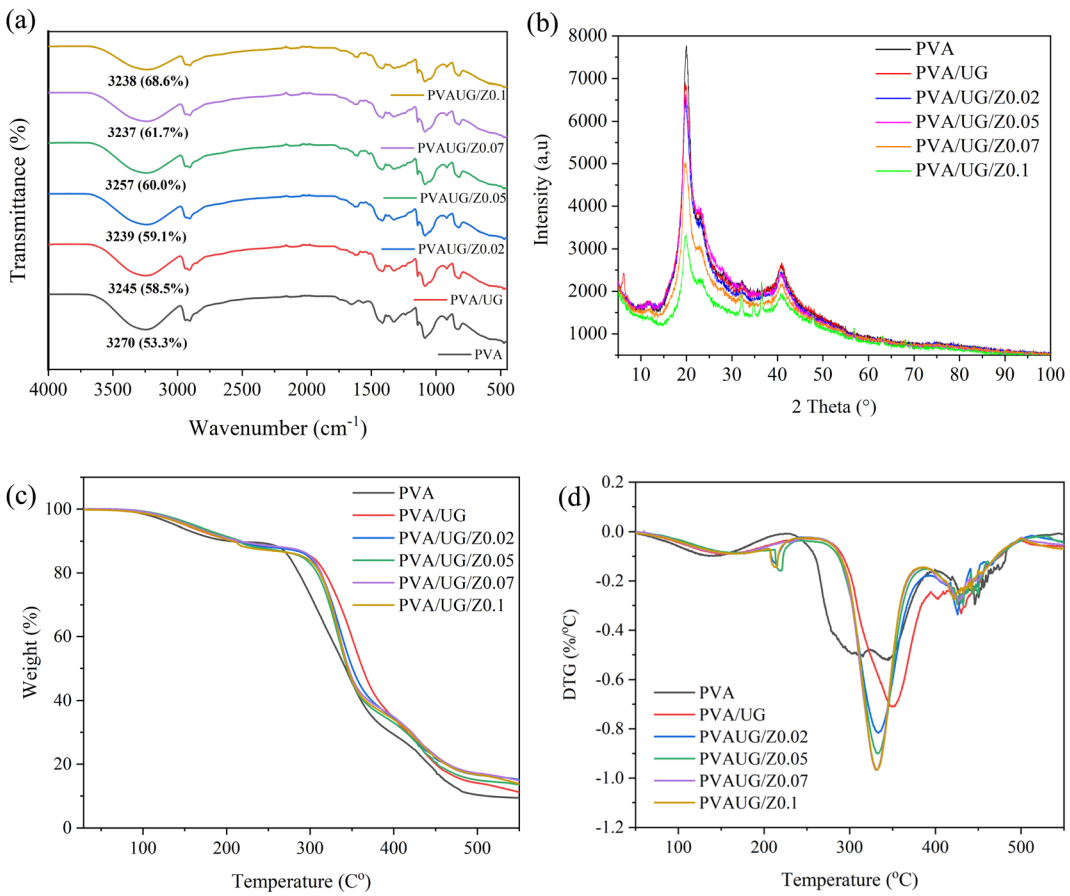

Fig. 2 FTIR (a), XRD (b), TGA (c), and DTG (d) curves for all samples.

and further with increasing concentrations of ZnO.[34] This reduction suggests that the incorporation of UG and ZnO into the PVA matrix may facilitate interactions or bonding that affect the ether or alcohol groups traditionally observed in PVA.[37]

The lowering of peak intensity in this region can be attributed to several potential mechanisms: the formation of new bonds involving these oxygen-containing groups, the physical encapsulation of these groups within the composite matrix, or chemical alterations such as cross-linking facilitated by ZnO. These interactions likely lead to a denser, more complex network within the material where the typical vibrational modes of the C–O groups are restricted, resulting in reduced peak intensities.[38]

XRD patterns for PVA films, in both their pure form and incorporated with UG and varying concentrations of ZnO, are shown in Fig. 2b. The XRD pattern for pure PVA shows sharp, well-defined peaks, reflecting its semi-crystalline nature, which is typical for untreated PVA films.[39] The addition of UG slightly alters these peaks, suggesting interactions that might affect the hydrogen bonding patterns within PVA, potentially due to the phenolic compounds present in UG.[40] Further structural changes are evident with the introduction of ZnO. As ZnO concentration increases (from 0.02 to 0.1), the XRD patterns display a shift in peak positions and a reduction in peak intensities.

The decreased peak intensity in the PVA/UG/ZnO films can be interpreted as a result of the capacity of ZnO nanoparticles to construct covalent bonds with the –OH groups of the PVA structure. According to Abd-Elnaiem *et al.*, this interaction facilitates crosslinking between the –OH groups of the PVA and the ZnO nanoparticles. Such crosslinking can significantly affect the material's mechanical properties and chemical stability.[41]

The TGA and DTG curves for the PVA, PVA/UG, and PVA/UG/ZnO films are shown in Fig. 2(c) and (d), respectively. The TGA curves demonstrate the thermal stability of the films, with all samples exhibiting a similar thermal degradation pattern. Pure PVA exhibits a two-step degradation process: the first weight loss occurs below 150 °C, attributed to the evaporation of water, while the second, with more significant weight loss, occurs between 300 °C and 400 °C, corresponding to the degradation of the PVA backbone.[42]

With the addition of UG, the thermal degradation pattern remains similar to that of pure PVA, but a slight improvement in thermal stability is observed. The onset of thermal degradation is delayed slightly, indicating that UG contributes to enhancing the thermal resistance of the composite.[43] However, the most noticeable improvement in thermal stability occurs with the incorporation of ZnO. As ZnO content increases, the onset temperature of the major degradation phase shifts towards higher temperatures. For example, the PVA/UG/Z0.1 film shows a delayed degradation onset compared to both pure PVA and PVA/UG. This enhancement in thermal stability can be attributed to the reinforcing effect of ZnO nanoparticles, which act as a barrier, preventing the diffusion of volatile degradation products and providing additional thermal protection to the polymer matrix.[44]

The DTG curves (Fig. 2d) further support these findings by showing the rate of weight loss as a function of temperature. Pure PVA exhibits a sharp DTG peak around 350 °C, indicating rapid degradation at this stage. With the addition of UG, the DTG peak shifts slightly to a higher temperature, while the incorporation of ZnO results in a more gradual degradation process, as indicated by the broader and less intense DTG peaks. This suggests that the ZnO particles help to reduce the thermal degradation process by stabilizing the polymer matrix.

3.2 Optical properties and surface characteristics

Fig. 3 illustrates the UV-vis transmittance properties of PVA films modified with UG and varying concentrations of ZnO, with a detailed analysis focused on the UVA (320–400 nm), UVB (280–320 nm), and blue light (400–495 nm) regions.[40] The transmittance curve for pure PVA (Fig. 1a) shows significant absorption in the UVB range. The curve indicates that pure PVA provides some protection against UVB although not as substantial as when additives are included. With the addition of UG (Fig. 1b), there is a marked improvement in UV blocking within the UVB and UVA ranges. This enhancement is attributed to the high content of phenolic compounds in UG, particularly catechins, which are known for their ability to absorb UV light. These compounds interact with the PVA matrix, which forms a network that dissipates UV radiation, thereby reducing transmittance. However, UG alone does not significantly enhance protection against blue light, as its absorption properties are more effective in the UV spectrum.[17,32]

The introduction of ZnO (Fig. 1c–f) further modifies the UV protection characteristics. Starting with a low concentration of ZnO (0.02), there is an interesting shift in the transmittance characteristics across both UVA and UVB regions. As the concentration of ZnO increases, the films exhibit a pronounced decrease, especially for blue light. Notably, samples containing 0.05, 0.07, and 0.1 wt% ZnO exhibit 100% UV and blue light blocking, with complete attenuation of wavelengths in the 400–495 nm range. This exceptional performance arises from ZnO's dual mechanisms: photon absorption within its wide band gap (~3.1 eV) and light scattering due to its nanoscale particle size and high refractive index. ZnO absorbs high-energy photons from UV and blue light, causing electron excitation from the valence band to the conduction band. This excitation generates electron–hole pairs that contribute to a denser optical barrier, effectively preventing light transmission.[44,45]

These findings underscore the synergistic effects of UG and ZnO in the composite matrix. UG primarily absorbs UV radiation, while ZnO extends protection into the blue light region through its bandgap properties and scattering capabilities. The dense composite structure formed by the interaction of these fillers with the PVA matrix further enhances the material's ability to block UV (UV-A and UV-B) and blue light. The result is a highly effective optical shield suitable for applications in protective coatings, packaging, and eyewear, where comprehensive protection against harmful wavelengths is crucial. However, the increased opacity in the visible range suggests a trade-off between UV protection and optical clarity,

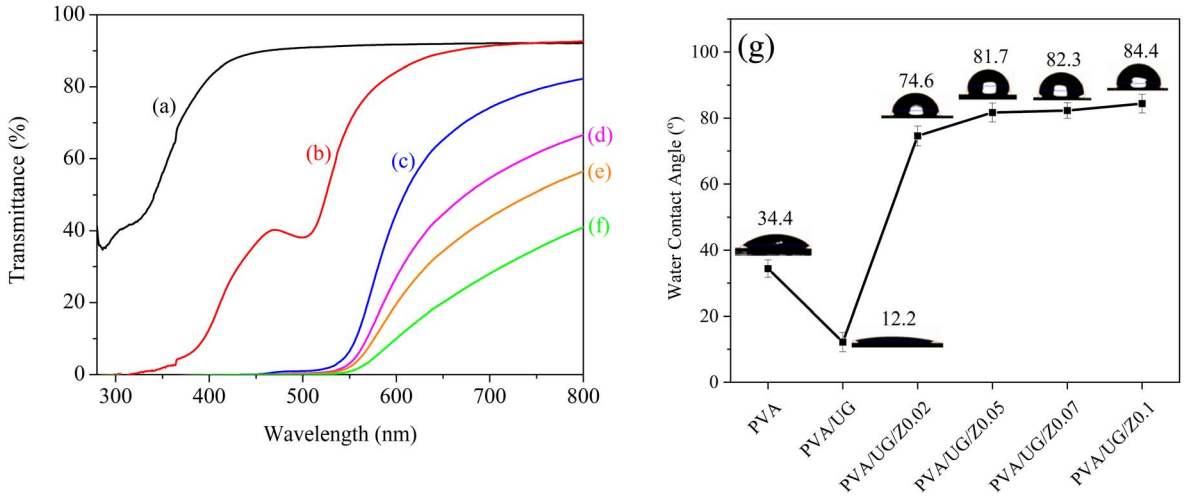

Fig. 3 UV-vis transmittance curves of PVA (a), PVA/UG (b), PVA/UG/Z0.02 (c), PVA/UG/Z0.05 (d), PVA/UG/Z0.07 (e), and PVA/UG/Z0.1 (f), and water contact angle values for all samples (g).

emphasizing the need for careful optimization of ZnO content depending on specific application requirements.

In addition to the UV-vis properties, the water contact angle (WCA) measurements further reveal the surface characteristics of the PVA/UG/ZnO films. As shown in Fig. 3g, the contact angle of pure PVA is 34.4°, indicating a relatively hydrophilic surface. Upon the incorporation of UG, the contact angle decreases significantly to 12.2°, suggesting a low performance of UG in enhancing the barrier properties of PVA, likely owing to the presence of polar groups in the UG. This is consistent with our previous work, which showed that the addition of UG does not significantly increase the contact angle value of PVA.[46] Interestingly, with the addition of ZnO, the water contact angle increases progressively with higher ZnO concentrations. For PVA/UG/ZnO films, the contact angle rises to 74.6° at 0.02 wt% ZnO and further increases to 84.4° at 0.1 wt% ZnO, indicating enhanced hydrophobicity. This increase in hydrophobicity with ZnO content can be attributed to surface roughness and the inherent hydrophobic nature of ZnO particles.[47] This result is consistent with the FTIR data, which show a reduction in the –OH stretch band intensity, suggesting fewer available hydroxyl groups as ZnO interacts with them, which contributes to the increased hydrophobicity.

3.3 Mechanical and morphological properties

The tensile properties of the PVA/UG/ZnO composite films were evaluated through the measurement of toughness (TN), elongation at break (EB), tensile strength (TS), and Young's modulus (YM), as illustrated in Fig. 4. The pure PVA sample, which serves as the control, showed moderate levels of TN, EB, TS, and YM, meaning that it has a good balance between flexibility and strength, but is not extremely strong or tough. When UG was added to PVA (PVA/UG), the film became more brittle, leading to lower toughness and elongation at break. However, both TS and YM increased compared to pure PVA. This suggests that while UG made the film stronger and stiffer, it also reduced its ability to stretch and absorb energy likely due to poor bonding between UG and PVA.

When ZnO was added to the PVA/UG composite (PVA/UG/Z), the mechanical properties improved noticeably. The addition of ZnO nanoparticles restored and enhanced both TN and EB, with the PVA/UG/Z0.1 sample showing the best performance. This improvement can be explained by the fact that ZnO acts as a reinforcing agent, helping to strengthen the material and allowing it to absorb more energy and stretch further without breaking. As more ZnO was added, TN and EB increased, showing that ZnO helped the film resist cracking and breaking better than PVA or PVA/UG alone.

Similarly, TS and YM also improved with the addition of ZnO. PVA/UG/Z composites, especially the sample with the highest ZnO content (PVA/UG/ZnO 0.1), showed the greatest increases in both strength and stiffness. This means that the material became stronger and more resistant to deformation as more ZnO was added. For the best-performing sample, PVA/UG/ZnO 0.1, the TS increased by approximately 56% compared to pure PVA, while the YM improved by 34%, showing significant enhancement in both strength and stiffness.

The addition of ZnO significantly improved the mechanical properties due to ZnO's role as a reinforcing filler. As observed by Huang *et al.*, ZnO promotes better polymer chain interactions, leading to stronger films. In the PVA/UG/Z, ZnO improved interfacial bonding and stress transfer, which increased the mechanical properties of the films through enhanced nanoparticle dispersion.[48] To further investigate the changes in mechanical behavior, Fig. 5 presents the FESEM images of the fractured surfaces of the films. The pure PVA film (Fig. 5a) exhibits a smooth and uniform surface, which is characteristic of its homogeneous structure. The addition of UG (Fig. 5b) introduces roughness and irregularities, indicating poor dispersion and weak bonding between the PVA matrix and UG, which contributes to the reduced energy absorption and brittleness observed during tensile testing.

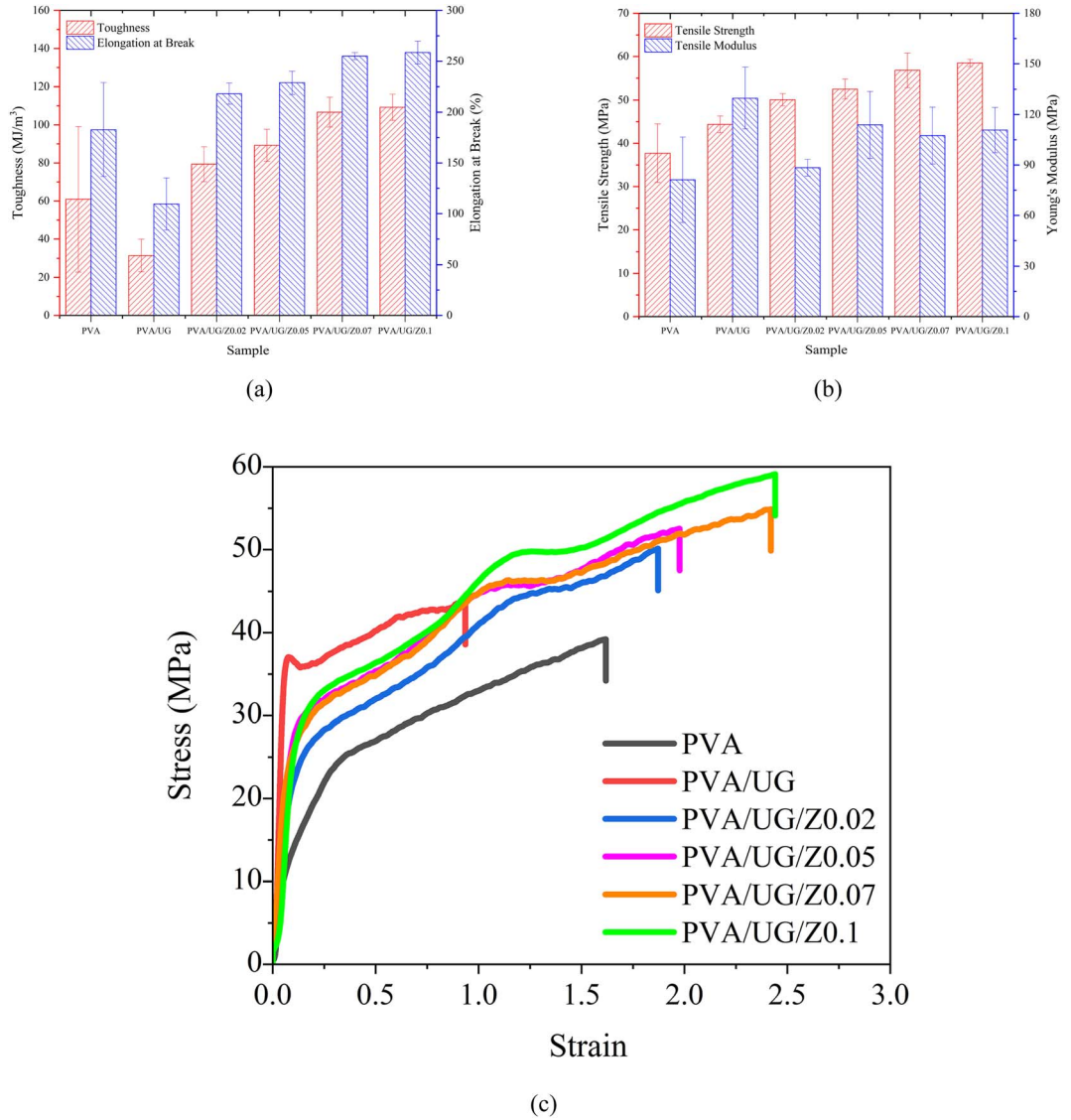

Fig. 4 Average values of TN-EB (a), TS-YM (b), and stress–strain curve (c) for all films.

At low ZnO concentrations (Fig. 5c), the fracture surface remains irregular, with no distinct ZnO nanoparticles visible. This might suggest that the nanoparticles are too small to be resolved at this composition. As the ZnO content increases to 0.05 wt% (Fig. 5d), the surface shows improved uniformity but still lacks clearly identifiable particles. In contrast, at higher ZnO concentrations (Fig. 5e and f), distinct ZnO nanoparticles are clearly visible as bright, irregular particles embedded within the PVA/UG matrix. Their presence indicates better nanoparticle dispersion and integration at these concentrations, likely contributing to enhanced mechanical performance. The nanoparticles act as stress transfer points, reinforcing the matrix and distributing applied loads more effectively.[49] This explains the significant improvement in toughness, elongation at break, tensile strength, and tensile modulus for these samples. For instance, PVA/UG/Z0.1, which shows the highest concentration of ZnO nanoparticles, achieved an 80% increase in TN and a 38% improvement in EB compared to pure PVA.

3.4 Durability and environmental impact

The moisture absorption data presented in Fig. 6a, and the water vapor permeability (WVP) and water vapor transmission (WVT) results shown in Fig. 6b together demonstrate the enhanced barrier properties of PVA/UG/ZnO composite films. In Fig. 6a, pure PVA exhibits the highest moisture absorption over the 480 minute testing period, which is consistent with its hydrophilic nature. The addition of UG slightly reduces moisture absorption, indicating some improvement in water resistance, although this effect remains moderate. The most significant reduction in moisture absorption occurs in the PVA/UG/ZnO composite films, particularly at higher ZnO concentrations, with the PVA/UG/Z0.1 film showing the lowest absorption. This is likely due to ZnO's ability to interact with hydroxyl (–OH) groups in PVA and UG, which reduces the number of free –OH groups available to bond with water molecules, thereby enhancing hydrophobicity.[41]

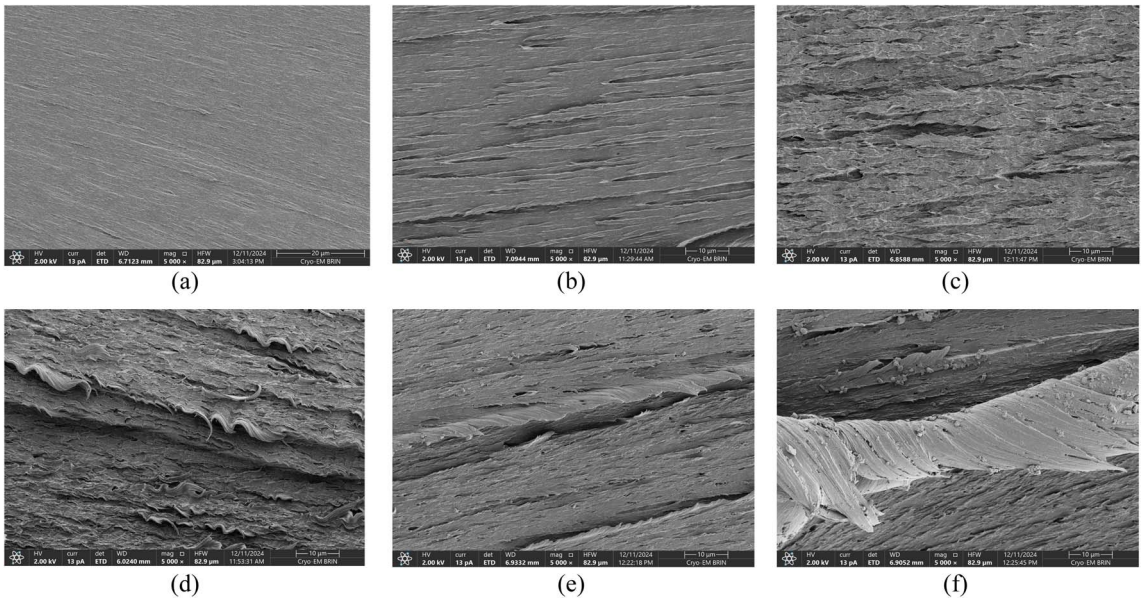

Fig. 5 Surface morphology of the film's fracture surface of PVA (a), PVA/UG (b), PVA/UG/Z0.02 (c), PVA/UG/Z0.05 (d), PVA/UG/Z0.07 (e), and PVA/UG/Z0.1 (f).

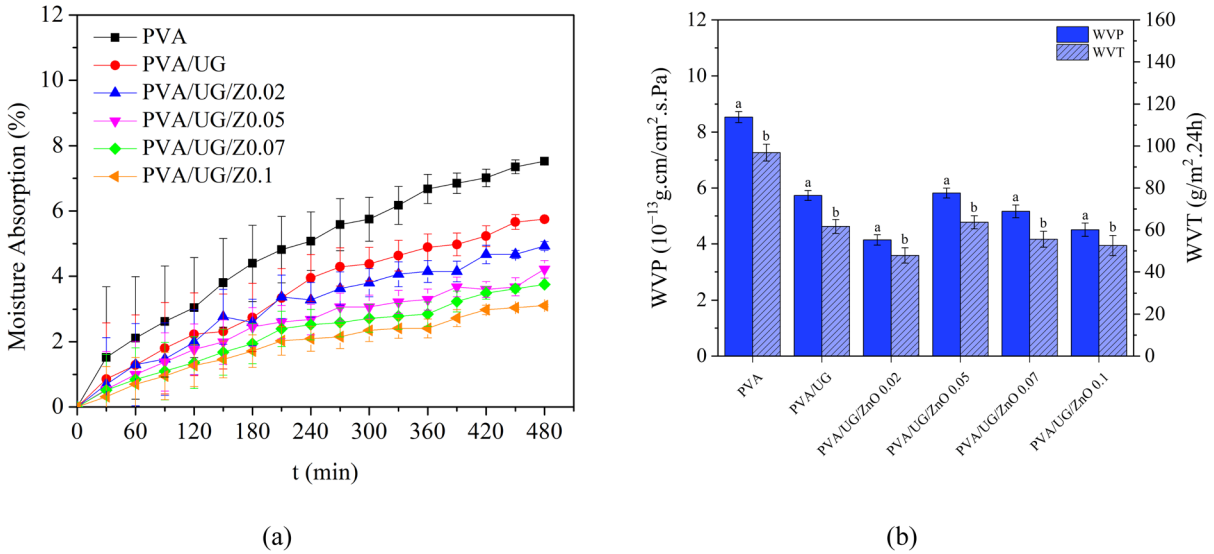

Fig. 6 Moisture absorption (a), and WVP-WVT (b) values for all films. Different lower-case letters indicate a significant difference in mean values ($p \leq 0.05$). Identical letters indicate values that are not significantly different.

Similarly, Fig. 6b shows that pure PVA also has the highest WVP and WVT, indicating greater water vapor permeability. The incorporation of UG reduces both WVP and WVT, improving the moisture barrier properties of the film, although not significantly. However, with the incremental addition of ZnO, WVP and WVT decrease substantially, with the PVA/UG/Z0.1 film again showing the lowest values. This reduction in permeability is attributed to ZnO's ability to form a denser composite structure, effectively hindering the movement of water vapor through the film.[50]

Table 1 provides a comparison of the WVP values from this work with the literature data. Notably, despite using only 0.02 wt% ZnO in the PVA/UG/ZnO films, the result is superior to or comparable with films from the literature that use much higher ZnO loadings. For instance, a PVA/ZnO film with 5 wt% ZnO exhibits a WVP of 1.61×10^{-13} g cm^{-1} cm^{-2} s^{-1} Pa^{-1}), which is lower than the current work's PVA/UG/ZnO films.[51] However, the films in this work achieve superior performance with far less ZnO, highlighting the synergy between ZnO and UG in enhancing barrier properties.

Additionally, when compared to other literature examples, the PVA/UG/Z0.02 film from this study demonstrates significantly better WVP. These results highlight the ability of UG to improve ZnO dispersion and interaction in the polymer matrix,

Table 1 Comparison of the WVP of this work's film with that reported in the literature

Films	ZnO (%)	WVP (g cm cm^{-2} s^{-1} Pa^{-1})	Ref.
PVA/ZnO/UG	0.02	4.14×10^{-13}	This work
PVA/ZnO	5	1.61×10^{-13}	51
PVA/graphene oxide/ZnO	5	1.94×10^{-9}	52
PVA/starch/ZnO	0.5	1.23×10^{-6}	53
PVA/gelatin/ZnO@quaternized chitosan	2	3.06×10^{-10}	54
PVA/glycerol/basil seed gum/ZnO	1	1.20×10^{-6}	55
Gelatin/cellulose nanofiber/ZnO	1	2.19×10^{-10}	29
Gelatin/tragacanth/ZnO	1	1.94×10^{-3}	28
Gelatin/mentha piperita/ZnO	5	4.52×10^{-8}	25

reducing the defects that facilitate water vapor transmission. Furthermore, the enhanced interaction between UG, ZnO, and PVA creates a dense, compact composite network that effectively blocks moisture movement.

In summary, Table 1 confirms that the PVA/UG/ZnO films in this work outperform films with similar ZnO loadings and achieve superior WVP with significantly lower ZnO concentrations compared to the literature. This demonstrates the remarkable efficiency of UG and ZnO in combination, making the films highly effective as moisture barriers.

3.5 Barrier and environmental resistance

The results from the soil burial test and antibacterial activity data illustrate the significant effects of ZnO concentration on the biodegradation and antibacterial properties of the PVA/UG/ZnO composite films. In the soil burial test (Fig. 7), the pure PVA film shows a steady increase in weight loss over the 30 day period, which indicates ongoing biodegradation. The addition of UG leads to even higher weight loss, especially on days 7 and 15, suggesting that UG enhances the biodegradability of the PVA matrix. However, as the concentration of ZnO increases, the weight loss progressively decreases, with the PVA/UG/Z0.1 sample exhibiting the least weight loss by day 30. This reduction in weight loss with a higher ZnO content suggests that ZnO enhances the structural integrity and durability of the films, slowing down their degradation in soil. This difference can be ascribed to the dense film structure mainly created by ZnO in the bulk phase of the film, thus delaying the degradation process. ZnO likely contributes to a denser matrix within the composite, reducing the access of microorganisms and moisture to the polymer chains, which results in decreased biodegradation rates.[56]

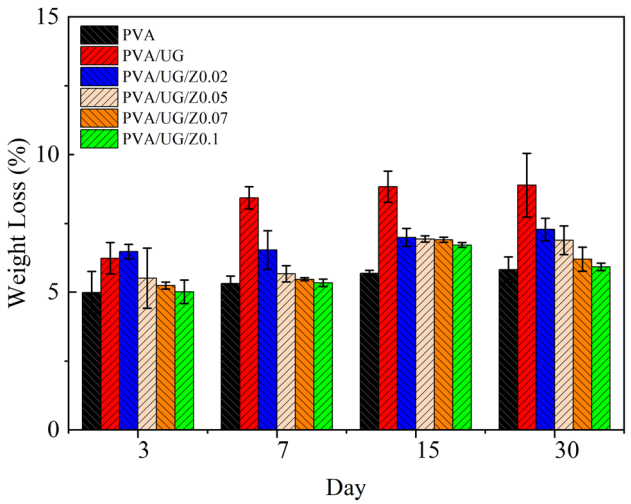

Fig. 7 Weight loss of all films in the soil burial test over a period of up to 30 days.

Fig. 8 demonstrates the antibacterial activity of the PVA/UG/ZnO films through the inhibition zones formed against *S. aureus* (Fig. 8a) and *E. coli* (Fig. 8b). As presented in Table 2, the addition of ZnO significantly enhances the antimicrobial performance of the films. The pure PVA/UG film does not exhibit any antibacterial effect, as shown by the absence of an inhibition zone. However, as ZnO is introduced and its concentration increases, the inhibition zone against *S. aureus* expands, with the PVA/UG/Z0.1 film showing the largest zone of inhibition (15.39 mm). Although the positive control (chloramphenicol disk) shows a larger inhibition zone, the ZnO-modified films demonstrate considerable antibacterial activity. For *E. coli*, no inhibition zone is observed for the PVA/UG film or the PVA/UG/Z0.02 film. However, with higher ZnO concentrations, the antibacterial activity against *E. coli* becomes significant. The PVA/UG/Z0.05 film exhibits an inhibition zone of 9.04 ± 0.32 mm, which further increases to 11.01 ± 0.45 mm in the PVA/UG/Z0.1 film.

This indicates a clear trade-off in the properties of the PVA/UG/ZnO films. As the ZnO content increases, the

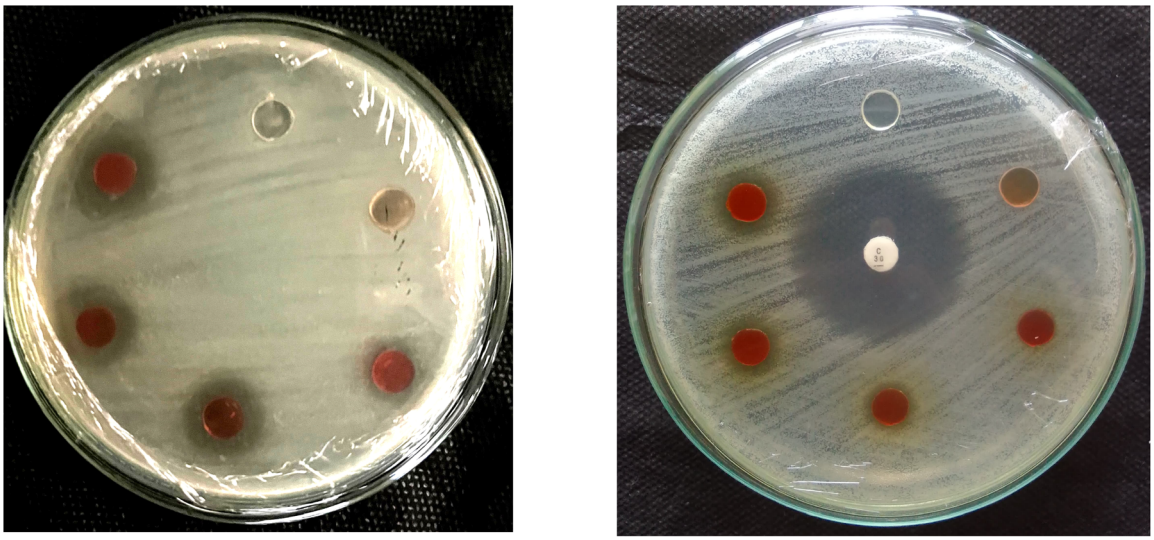

(a) (b)

Fig. 8 Diameter of the inhibition zone represented by a more transparent area against (a) *S. aureus* and (b) *E. coli*.

Table 2 Antimicrobial activity of all samples

No.	Sample	Diameter of inhibition zone (mm) against *S. aureus*	Diameter of inhibition zone (mm) against *E. coli*
1	PVA/UG	—	0
2	PVA/UG/Z0.02	11.14 ± 0.20	0
3	PVA/UG/Z0.05	13.43 ± 1.45	9.04 ± 0.32
4	PVA/UG/Z0.07	14.74 ± 1.93	8.96 ± 0.73
5	PVA/UG/Z0.1	15.39 ± 1.60	11.01 ± 0.45
6	Positive control (+)chloramphenicol disk 30 μg per disk	28.97 ± 0.99	31.61 ± 0.17

biodegradability of the films decreases owing to enhanced structural integrity and reduced degradation in soil. However, higher ZnO concentrations significantly improve the antibacterial properties of the films, making them more effective against *S. aureus*. Therefore, the choice of ZnO concentration in these films must balance the need for biodegradability with the requirement for antibacterial performance depending on the intended application.

4. Conclusions

This study successfully developed and characterized PVA composite films integrated with UG and ZnO as fillers. The incorporation of ZnO and UG into the PVA matrix resulted in substantial improvements in UV and blue light shielding. UV-vis spectrophotometry revealed that films containing 0.05, 0.07, and 0.1 wt% ZnO exhibited 100% UV and blue light blocking. Additionally, the composite films displayed enhanced mechanical properties, with tensile strength increasing by 56% and elasticity improving by 38% compared to pure PVA, highlighting ZnO's role as a reinforcing agent. Surface characterization, including water contact angle measurements, showed a marked increase in hydrophobicity with the addition of ZnO. The water contact angle improved from 34.4° for pure PVA to 84.4° for PVA/UG/ZnO composites with 0.1 wt% ZnO, indicating that these composite films have potential applications in environments requiring moisture resistance. The reduction in –OH group availability, as observed in the FTIR spectra, supported this finding, which suggests that ZnO interacts with hydroxyl groups, contributing to the enhanced hydrophobicity and barrier properties of the films.

However, a trade-off between biodegradability and antibacterial efficacy was observed. The soil burial test demonstrated that although UG improves the biodegradability of the PVA films, the addition of ZnO progressively reduced the weight loss, indicating a decrease in biodegradability. This reduction is likely due to the denser structure formed by ZnO, which impedes the penetration of microorganisms and moisture into the polymer matrix, thereby reducing degradation. In contrast, the antibacterial activity of the films improved significantly with higher ZnO concentrations. Against *S. aureus*, the inhibition zone increased from 11.14 mm for PVA/UG/Z0.02 to 15.39 mm for PVA/UG/Z0.1. Similarly, against *E. coli*, the inhibition zone increased from 9.04 ± 0.32 mm for PVA/UG/Z0.05 to 11.01 ± 0.45 mm for PVA/UG/Z0.1.

In conclusion, the PVA/UG/ZnO composite films offer a balance of UV protection, mechanical strength, hydrophobicity, and antibacterial properties, with the trade-off between

biodegradability and durability being a key consideration. These findings open pathways for further exploration of these films in applications such as sustainable packaging and protective eyewear, where UV shielding, moisture resistance, and antibacterial effectiveness are critical. Future work should focus on optimizing ZnO content to strike the right balance between environmental sustainability and performance depending on the specific application.

Data availability

The data supporting the findings of this study are available from the corresponding author upon reasonable request.

Author contributions

Dieter Rahmadiawan: validation, formal analysis, investigation, writing – original draft Hairul Abral: conceptualization, methodology, supervision, resources, writing – review & editing, funding acquisition. Muhammad Aldi Pratama: investigation, visualization, data curation Hyun-Joong Kim: investigation Razan Muhammad Railis: investigation, Software Robi Kurniawan: investigation, writing – review & editing Sri Rizki Putri Primandari: writing – review & editing Shih-Chen Shi: resources, validation Melbi Mahardika: investigation.

Conflicts of interest

There are no conflicts to declare.

Acknowledgements

This work was supported by the Universitas Andalas for supporting research funding with project name Riset Kolaborasi Indonesia (RKI) Skema C (Host), number: 10/UN16.19/PT.01.03/RKI/2024.

References

1 I. V Ivanov, T. Mappes, P. Schaupp, C. Lappe and S. Wahl, Ultraviolet radiation oxidative stress affects eye health, *J. Biophotonics*, 2018, **11**, e201700377, DOI: **10.1002/jbio.201700377**.

2 M. I. Silvani, R. Werder and C. Perret, The influence of blue light on sleep, performance and wellbeing in young adults: a systematic review, *Front. Physiol.*, 2022, **13**, 943108, DOI: **10.3389/fphys.2022.943108**). **https://www.frontiersin.org/journals/physiology/articles/10.3389/fphys.2022.943108**.

3 A. Cougnard-Gregoire, B. M. J. Merle, T. Aslam, J. M. Seddon, I. Aknin, C. C. W. Klaver, G. Garhöfer, A. G. Layana, A. M. Minnella, R. Silva and C. Delcourt, Blue Light Exposure: Ocular Hazards and Prevention—A Narrative Review, *Ophthalmol. Ther.*, 2023, **12**, 755–788, DOI: **10.1007/s40123-023-00675-3**.

4 J. A. Yoo, E. Yu, S.-H. Park, S. W. Oh, K. Kwon, S. J. Park, H. Kim, S. Yang, J. Y. Park, J. Y. Cho, Y.-J. Kim and J. Lee, Blue Light Irradiation Induces Human Keratinocyte Cell Damage *via* Transient Receptor Potential Vanilloid 1 (TRPV1) Regulation, *Oxid. Med. Cell. Longev.*, 2020, **2020**, 8871745, DOI: **10.1155/2020/8871745**.

5 M. F. Holick, Sunlight, UV Radiation, Vitamin D, and Skin Cancer: How Much Sunlight Do We Need? BT - Sunlight, Vitamin D and Skin Cancer, in *Sunlight, Vitam. D Ski. Cancer*. ed. J. Reichrath, Springer International Publishing, Cham, 2020, pp. 19–36, DOI: **10.1007/978-3-030-46227-7_2**.

6 D. Rahmadiawan and S.-C. Shi, Enhanced Stability, Superior Anti-Corrosive, and Tribological Performance of Al_2O_3 Water-based Nanofluid Lubricants with Tannic Acid and Carboxymethyl Cellulose over SDBS as Surfactant, *Sci. Rep.*, 2024, **14**, 9217, DOI: **10.1038/s41598-024-59010-w**.

7 D. Rahmadiawan, S. C. Shi, Z. Fuadi, H. Abral, N. Putra, R. Irwansyah, D. Gasni and A. M. Fathoni, Experimental investigation on stability, tribological, viscosity, and thermal conductivity of MXene/Carboxymethyl cellulose (CMC) water-based nanofluid lubricant, *J. Tribol.*, 2023, **39**, 36–50.

8 S.-C. Shi, C.-F. Hsieh and D. Rahmadiawan, Enhancing mechanical properties of polylactic acid through the incorporation of cellulose nanocrystals for engineering plastic applications, *Teknomekanik*, 2024, **7**(1), 20–28, DOI: **10.24036/teknomekanik.v7i1.30072**.

9 S. C. Shi, F. I. Lu, C. Y. Wang, Y. T. Chen, K. W. Tee, R. C. Lin, H. L. Tsai and D. Rahmadiawan, Rice straw-derived chitosan-enhanced plasticizers as biologically and environmentally friendly alternatives for sustainable materials, *Int. J. Biol. Macromol.*, 2024, **264**, 130547, DOI: **10.1016/j.ijbiomac.2024.130547**.

10 E. Hakiim, H. Nurdin, Z. Abadi and W.-T. Zhuang, Tensile strength study of mensiang (scirpuss grossus) fibre composites with unsaturated polyester resin matrix, *Journal of Engineering Researcher and Lecturer*, 2024, **4**(1), 1–8, DOI: **10.58712/jerel.v3i3.164**.

11 D. V. Francis, S. Thaliyakattil, L. Cherian, N. Sood and T. Gokhale, Metallic Nanoparticle Integrated Ternary Polymer Blend of PVA/Starch/Glycerol: A Promising Antimicrobial Food Packaging Material, *Polymers*, 2022, **14**(7), 1379, DOI: **10.3390/polym14071379**.

12 Z. Li, W. Xu, X. Wang, W. Jiang, X. Ma, F. Wang, C. Zhang and C. Ren, Fabrication of PVA/PAAm IPN hydrogel with high adhesion and enhanced mechanical properties for body sensors and antibacterial activity, *Eur. Polym. J.*, 2021, **146**, 110253, DOI: **10.1016/j.eurpolymj.2020.110253**.

13 D. Rahmadiawan, S.-C. Shi and W.-T. Zhuang, Reinforcing polyvinyl alcohol films with layered double hydroxide and tannic acid to enhance tensile strength, tribological performance, and corrosion resistance in biomedical coating applications, *Mater. Res. Express*, 2024, **11**, 115302, DOI: **10.1088/2053-1591/ad8f94**.

14 K. Palanichamy, M. Anandan, J. Sridhar, V. Natarajan and A. Dhandapani, PVA and PMMA nano-composites: a review on strategies, applications and future prospects, *Mater. Res. Express*, 2023, **10**, 22002, DOI: **10.1088/2053-1591/acb527**.

15 A. Rauf, Rahmawaty and A. Z. Siregar, The Condition of *Uncaria gambir Roxb.* as One of Important Medicinal Plants in North Sumatra Indonesia, *Procedia Chem.*, 2015, **14**, 3–10, DOI: 10.1016/j.proche.2015.03.002.

16 T.-J. Ho, P.-H. Tsai, C.-H. Hsieh, J.-H. Lin, Y.-W. Lin, J.-R. Wu and H.-P. Chen, Role of Herbal Extracts of Catechu from *Uncaria gambir* in the Treatment of Chronic Diabetic Wounds, *Pharmaceuticals*, 2022, **16**, 66, DOI: 10.3390/ph16010066.

17 D. Rahmadiawan, H. Abral, M. K. Ilham, P. Puspitasari, R. A. Nabawi, S. C. Shi, E. Sugiarti, A. N. Muslimin, D. Chandra, R. A. Ilyas and R. Zainul, Enhanced UV blocking, tensile and thermal properties of bendable TEMPO-oxidized bacterial cellulose powder-based films immersed in PVA/*Uncaria gambir*/ZnO solution, *J. Mater. Res. Technol.*, 2023, **26**, 5566–5575, DOI: 10.1016/j.jmrt.2023.08.267.

18 I. P. Munggari, D. Kurnia, Y. Deawati and E. Julaeha, Current Research of Phytochemical, Medicinal and Non-Medicinal Uses of *Uncaria gambir roxb.*: A Review, *Molecules*, 2022, **27**(19), 6551, DOI: 10.3390/molecules27196551.

19 J. Xu, Y. Zhang, Y. Gutha and W. Zhang, Antibacterial property and biocompatibility of Chitosan/Poly(vinyl alcohol)/ZnO (CS/PVA/ZnO) beads as an efficient adsorbent for Cu(II) removal from aqueous solution, *Colloids Surf., B*, 2017, **156**, 340–348, DOI: 10.1016/j.colsurfb.2017.05.028.

20 W. J. Chong, S. Shen, Y. Li, A. Trinchi, D. Pejak Simunec, I. Kyratzis, A. Sola and C. Wen, Biodegradable PLA-ZnO nanocomposite biomaterials with antibacterial properties, tissue engineering viability, and enhanced biocompatibility, *Smart Mater. Manuf.*, 2023, **1**, 100004, DOI: 10.1016/j.smmf.2022.100004.

21 H. M. Tun, R. E. Wulansari, D. Pradhan and Z. M. Naing, Design, fabrication and measurement of metal-semiconductor field effect transistor based on zinc oxide material, *J. Eng. Res. Lect.*, 2023, **2**, 104–111, DOI: 10.58712/jerel.v2i3.103.

22 N. Asif, M. Amir and T. Fatma, Recent advances in the synthesis, characterization and biomedical applications of zinc oxide nanoparticles, *Bioprocess Biosyst. Eng.*, 2023, **46**, 1377–1398, DOI: 10.1007/s00449-023-02886-1.

23 S. Jha, R. Rani and S. Singh, Biogenic Zinc Oxide Nanoparticles and Their Biomedical Applications: A Review, *J. Inorg. Organomet. Polym. Mater.*, 2023, **33**, 1437–1452, DOI: 10.1007/s10904-023-02550-x.

24 B. Meindrawan, S. Putri, C. S. Susanto, O. Ofe, D. Mangindaan, A. Ayman and T. P. Kasih, Bionanocomposite of Gelatin–ZnO Nanoparticles as Potential Edible Coating for Broiler Chicken Fillet, *Macromol. Symp.*, 2020, **391**, 1–6, DOI: 10.1002/masy.201900165.

25 S. Javidi, A. Mohammadi Nafchi and H. H. Moghadam, Synergistic effect of nano-ZnO and Mentha piperita essential oil on the moisture sorption isotherm, antibacterial activity, physicochemical, mechanical, and barrier properties of gelatin film, *J. Food Meas. Charact.*, 2022, **16**, 964–974, DOI: 10.1007/s11694-021-01217-w.

26 M. I. H. Mondal, M. M. Islam and F. Ahmed, Enhanced wound healing with biogenic zinc oxide nanoparticle-incorporated carboxymethyl cellulose/polyvinylpyrrolidone nanocomposite hydrogels, *Biomater. Sci.*, 2025, **13**, 193–209, DOI: 10.1039/D4BM01027B.

27 X. Sun, H. Wang, H. Liang, N. Meng and N. Zhou, Fabrication of antimicrobial chitosan/ZnO nanoparticles/lecithin-montmorillonite films for food packaging application, *Food Hydrocoll.*, 2025, **159**, 110686, DOI: 10.1016/j.foodhyd.2024.110686.

28 R. Shahvalizadeh, R. Ahmadi, I. Davandeh, A. Pezeshki, S. A. Seyed Moslemi, S. Karimi, M. Rahimi, H. Hamishehkar and M. Mohammadi, Antimicrobial bio-nanocomposite films based on gelatin, tragacanth, and zinc oxide nanoparticles – Microstructural, mechanical, thermo-physical, and barrier properties, *Food Chem.*, 2021, **354**, 129492, DOI: 10.1016/j.foodchem.2021.129492.

29 A. Ahmadi, P. Ahmadi, M. A. Sani, A. Ehsani and B. Ghanbarzadeh, Functional biocompatible nanocomposite films consisting of selenium and zinc oxide nanoparticles embedded in gelatin/cellulose nanofiber matrices, *Int. J. Biol. Macromol.*, 2021, **175**, 87–97, DOI: 10.1016/j.ijbiomac.2021.01.135.

30 W. Liu, T. Wang, Y. Tao, Z. Ling, C. Huang, C. Lai and Q. Yong, Fabrication of anti-bacterial, hydrophobic and UV resistant galactomannan-zinc oxide nanocomposite films, *Polymer*, 2021, **215**, 123412, DOI: 10.1016/j.polymer.2021.123412.

31 D. Rahmadiawan, H. Abral, R. M. Railis, I. C. Iby, M. Mahardika, D. Handayani, K. D. Natrana, D. Juliadmi and F. Akbar, The Enhanced Moisture Absorption and Tensile Strength of PVA/*Uncaria gambir* Extract by Boric Acid as a Highly Moisture-Resistant, Anti-UV, and Strong Film for Food Packaging Applications, *J. Compos. Sci.*, 2022, **6**, 337, DOI: 10.3390/jcs6110337.

32 H. Abral, M. Ikhsan, D. Rahmadiawan, D. Handayani, N. Sandrawati, E. Sugiarti and A. Novi, Anti-UV, antibacterial, strong, and high thermal resistant polyvinyl alcohol/*Uncaria gambir* extract biocomposite film, *J. Mater. Res. Technol.*, 2022, **17**, 2193–2202, DOI: 10.1016/j.jmrt.2022.01.120.

33 Z. Zhao, A. Mao, W. Gao and H. Bai, A facile *in situ* method to fabricate transparent, flexible polyvinyl alcohol/ZnO film for UV-shielding, *Compos. Commun.*, 2018, **10**, 157–162, DOI: 10.1016/j.coco.2018.09.009.

34 L. Yang, L. Ren, Y. Zhao, S. Liu, H. Wang, X. Gao, B. Niu and W. Li, Preparation and characterization of PVA/arginine chitosan/ZnO NPs composite films, *Int. J. Biol. Macromol.*, 2023, **226**, 184–193, DOI: 10.1016/j.ijbiomac.2022.12.020.

35 M. S. Sarwar, M. B. K. Niazi, Z. Jahan, T. Ahmad and A. Hussain, Preparation and characterization of PVA/nanocellulose/Ag nanocomposite films for antimicrobial food packaging, *Carbohydr. Polym.*, 2018, **184**, 453–464, DOI: 10.1016/j.carbpol.2017.12.068.

36 H. Noei, H. Qiu, Y. Wang, E. Löffler, C. Wöll and M. Muhler, The identification of hydroxyl groups on ZnO nanoparticles

by infrared spectroscopy, *Phys. Chem. Chem. Phys.*, 2008, **10**, 7092–7097, DOI: 10.1039/B811029H.

37 Y. Köse, E. Suvacı and B. Atlı, Improving properties of biodegradable chitosan/PVA composite polymers *via* novel designed ZnO particles, *J. Aust. Ceram. Soc.*, 2023, **59**, 245–257, DOI: 10.1007/s41779-022-00830-2.

38 P. Yadav, V. Lahariya, P. P. Pandey, S. Behl and R. Raghav, Investigation of thermal and dielectric behaviour of PVA–ZnO nanocomposite films, *J. Mater. Sci. Mater. Electron.*, 2023, **34**, 787, DOI: 10.1007/s10854-023-10178-3.

39 A. M. Hezma, A. Rajeh and M. A. Mannaa, An insight into the effect of zinc oxide nanoparticles on the structural, thermal, mechanical properties and antimicrobial activity of Cs/PVA composite, *Colloids Surf., A*, 2019, **581**, 123821, DOI: 10.1016/j.colsurfa.2019.123821.

40 S. Zeng, X. Liu, J. Li, H. Zhao, D. Guo and X. Tong, Multi-functional polyvinyl alcohol/tannin acid composite films incorporated with lignin nanoparticles loaded by potassium sorbate, *Int. J. Biol. Macromol.*, 2024, **264**, 130474, DOI: 10.1016/j.ijbiomac.2024.130474.

41 A. M. Abd-Elnaiem, M. Rashad, T. A. Hanafy and N. M. Shaalan, Improvement of Optical Properties of Functionalized Polyvinyl Alcohol-Zinc Oxide Hybrid Nanocomposites for Wide UV Optoelectronic Applications, *J. Inorg. Organomet. Polym. Mater.*, 2023, **33**, 2429–2444, DOI: 10.1007/s10904-023-02616-w.

42 W. Yang, H. Ding, G. Qi, C. Li, P. Xu, T. Zheng, X. Zhu, J. M. Kenny, D. Puglia and P. Ma, Highly transparent PVA/nanolignin composite films with excellent UV shielding, antibacterial and antioxidant performance, *React. Funct. Polym.*, 2021, **162**, 104873, DOI: 10.1016/j.reactfunctpolym.2021.104873.

43 A. P. Wardana, N. S. Aminah, A. N. Kristanti, M. Z. Fahmi, H. I. Zahrah, W. Widiyastuti, H. A. Ajiz, U. Zubaidah, P. A. Wiratama and Y. Takaya, Nano *Uncaria gambir* as Chemopreventive Agent Against Breast Cancer, *Int. J. Nanomed.*, 2023, **18**, 4471–4484, DOI: 10.2147/IJN.S403385.

44 I. A. Channa, J. Ashfaq, S. J. Gilani, A. A. Shah, A. D. Chandio and M. N. Bin Jumah, UV Blocking and Oxygen Barrier Coatings Based on Polyvinyl Alcohol and Zinc Oxide Nanoparticles for Packaging Applications, *Coatings*, 2022, **12**(7), 897, DOI: 10.3390/coatings12070897.

45 H. Premkumar, Synthesis, characterization and photocatalytic performance of polyvinyl alcohol/zinc oxide nanocomposites: A comprehensive study, *Nano-Struct. Nano-Objects*, 2024, **39**, 101208, DOI: 10.1016/j.nanoso.2024.101208.

46 D. Rahmadiawan, H. Abral, I. Chayri Iby, H. J. Kim, K. H. Ryu, H. W. Kwack, M. Razan Railis, E. Sugiarti, A. Novi Muslimin, D. Handayani, K. Dwinatrana, S. C. Shi, R. Zainul and R. Azis Nabawi, Effect of post-heat treatment on the UV transmittance, hydrophobicity, and tensile properties of PVA/*Uncaria gambir* extract blend films, *Heliyon*, 2024, **10**, e30748, DOI: 10.1016/j.heliyon.2024.e30748.

47 M. Q. Khan, D. Kharaghani, N. Nishat, A. Shahzad, T. Hussain, Z. Khatri, C. Zhu and I. S. Kim, Preparation and characterizations of multifunctional PVA/ZnO nanofibers composite membranes for surgical gown application, *J. Mater. Res. Technol.*, 2019, **8**, 1328–1334, DOI: 10.1016/j.jmrt.2018.08.013.

48 X. Huang, X. Zhou, Q. Dai and Z. Qin, Antibacterial, Antioxidation, UV-Blocking, and Biodegradable Soy Protein Isolate Food Packaging Film with Mangosteen Peel Extract and ZnO Nanoparticles, *Nanomaterials*, 2021, **11**(12), 3337, DOI: 10.3390/nano11123337.

49 D. Rahmadiawan, H. Abral, W. H. Yesa, D. Handayani, N. Sandrawati, E. Sugiarti, A. N. Muslimin, S. M. Sapuan and R. A. Ilyas, White Ginger Nanocellulose as Effective Reinforcement and Antimicrobial Polyvinyl Alcohol/ZnO Hybrid Biocomposite Films Additive for Food Packaging Applications, *J. Compos. Sci.*, 2022, **6**, 316, DOI: 10.3390/jcs6100316.

50 I. M. Factori, J. M. Amaral, P. H. Camani, D. S. Rosa, B. A. Lima, M. Brocchi, E. R. da Silva and J. S. Souza, ZnO Nanoparticle/Poly(vinyl alcohol) Nanocomposites *via* Microwave-Assisted Sol–Gel Synthesis for Structural Materials, UV Shielding, and Antimicrobial Activity, *ACS Appl. Nano Mater.*, 2021, **4**, 7371–7383, DOI: 10.1021/acsanm.1c01334.

51 E. Gharoy Ahangar, M. H. Abbaspour-Fard, N. Shahtahmassebi, M. Khojastehpour and P. Maddahi, Preparation and Characterization of PVA/ZnO Nanocomposite, *J. Food Process. Preserv.*, 2015, **39**, 1442–1451, DOI: 10.1111/jfpp.12363.

52 R. Zhang, Y. Wang, D. Ma, S. Ahmed, W. Qin and Y. Liu, Effects of ultrasonication duration and graphene oxide and nano-zinc oxide contents on the properties of polyvinyl alcohol nanocomposites, *Ultrason. Sonochem.*, 2019, **59**, 104731, DOI: 10.1016/j.ultsonch.2019.104731.

53 W. Hu, Z. Zou, H. Li, Z. Zhang, J. Yu and Q. Tang, Fabrication of highly transparent and multifunctional polyvinyl alcohol/starch based nanocomposite films using zinc oxide nanoparticles as compatibilizers, *Int. J. Biol. Macromol.*, 2022, **204**, 284–292, DOI: 10.1016/j.ijbiomac.2022.02.020.

54 K. Wang, X. Yang, J. Liang, Y. Rong, W. Zhao, J. Ding, Y. Liu and Q. Liu, Preparation, characterization, antimicrobial evaluation, and grape preservation applications of polyvinyl alcohol/gelatin composite films containing zinc oxide@quaternized chitosan nanoparticles, *Int. J. Biol. Macromol.*, 2024, **277**, 134527, DOI: 10.1016/j.ijbiomac.2024.134527.

55 S.-M. Hasheminya, J. Dehghannya and A. Ehsani, Development of basil seed mucilage (a heteropolysaccharide) – Polyvinyl alcohol biopolymers incorporating zinc oxide nanoparticles, *Int. J. Biol. Macromol.*, 2023, **253**, 127342, DOI: 10.1016/j.ijbiomac.2023.127342.

56 Y. Xie, Y. Pan and P. Cai, Cellulose-based antimicrobial films incroporated with ZnO nanopillars on surface as biodegradable and antimicrobial packaging, *Food Chem.*, 2022, **368**, 130784, DOI: 10.1016/j.foodchem.2021.130784.